scientific reports

Check for updates

OPEN

Study on the mechanical properties and microscopic mechanism of xanthan gum improved red clay

Fan Yang[1], Zhixia Zhao[1]✉, Zhaoying Jia[1], Wangjin Niu[2]✉, Yongxia Liu[3], Fuyong Song[4], Huanyu Dong[5] & Hongji Deng[2]

To mitigate the adverse ecological impacts of inorganic solidified materials on modified red clay and address the issues of low bearing capacity and extensive cracking under hydraulic erosion, this study investigates the use of low-environmental-impact materials to improve the mechanical fracturing of red clay. In this context, this study focuses on modifying red clay using an environmentally friendly biopolymer, xanthan gum (XG). Through a series of laboratory mechanical and microstructural tests, the effects of XG on the mechanical fracturing, California Bearing Ratio (CBR), and microstructural characteristics of red clay are examined. The results indicate that the shear strength of XG-modified red clay increases approximately linearly with the increase in normal stress. The cohesion and internal friction angle of the modified soil first increase and then decrease with the increasing XG dosage. The compressive strength of the modified soil initially increases and then decreases with the addition of XG, with the most rapid growth occurring between 14 and 28 days. The deformation modulus of the modified soil initially increases and then decreases with increasing XG dosage, achieving a 7.71% increase after 28 days. As the number of cycles increases, the development of fractures in the modified soil slows down, primarily due to the transformation of secondary fractures into primary fractures. The internal friction angle of the modified soil decreases with the increasing number of cycles, while the cohesion and compressive strength exhibit a decreasing trend. The CBR of the modified soil first increases and then decreases with the increasing XG dosage, reaching a peak value of 24.1%. The addition of XG promotes the formation of flake-like and needle-like polymer bonding products that cover the soil particles, fill the pores, and form dense aggregates. After 28 days, the hydrophilic minerals in the modified soil decreased by 53.99%. Pore analysis reveals a decrease in the average porosity and total pore volume of the XG-modified soil. The research results provide a novel modification approach to address the ecological environmental issues associated with the treatment of red clay using inorganic solidifiers, offering valuable numerical references for similar engineering projects.

Keywords Red clay and xanthan gum (XG), Mechanical fracturing, California bearing ratio (CBR), Wetting-drying cycle, Microstructural features

Red clay refers to a special type of clay formed from the natural weathering of certain saline rocks under alternating wet and hot conditions, characterized by its high liquid limit[1]. It is notable for its high plasticity, high water content, high void ratio, and low density[2], and is widely distributed in the Yunnan-Guizhou, Guangxi-Guangdong, and Hunan-Hubei provinces of China. Red clay exhibits the properties of "softening upon water absorption and cracking upon water loss"[3]. The Hubei-Hunan provinces in China experiences high rainfall, and red clay is highly sensitive to water. Furthermore, changes in the surrounding environment, temperature, and humidity significantly impact on the engineering properties of red clay. These characteristics often lead to engineering problems such as pavement cracking, subsidence, slope cracking, shallow landslides, and insufficient foundation bearing capacity[4]. The strength of red clay decreases rapidly upon water absorption, resulting in soil shrinkage and cracking. These engineering issues associated with the unique properties of red clay led to increased construction costs, severely affecting the safety of local residents[5], and caused significant economic

[1]Shandong Labor Vocational and Technical College, Jinan 250300, China. [2]School of Civil Engineering, Architecture and Environment, Hubei University of Technology, Wuhan 430068, China. [3]Gansu Tieke Construction Engineering Consulting Co., Ltd., Lanzhou 730030, China. [4]Nanjing Dongzhong Construction Engineering Co, Nanjing 211313, China. [5]Power Construction Corporation of China, Xi An 712000, China. ✉email: 455935137@qq.com; 3027607847@qq.com

losses due to geological disasters. They also pose threats to the safety and stability of infrastructure. Therefore, to accelerate high-quality socio-economic development and ensure the stability of urban infrastructure, it is urgent to address the engineering problems caused by the unique properties of red clay[6].

In response to the engineering particularities of red clay, it is generally not suitable for direct use as a subgrade filler. Stabilization treatments are commonly required prior to construction, including physical and chemical modifications. Chemical stabilization typically involves the addition of lime or cement[7], which can enhance the engineering properties of red clay. However, these methods are often limited to small-scale applications and may yield suboptimal results due to issues such as non-uniform mixing. Physical stabilization, such as the incorporation of fibers[8,9], can improve tensile and shear strength and form a network that inhibits the expansion and contraction of red clay. However, fibers are highly susceptible to degradation over time, leading to performance failure. With the advancement of ecological and environmental construction, researchers have begun to explore biopolymers as red clay stabilizers. Compared to conventional chemical and physical stabilization methods, biopolymers offer an eco-friendly, sustainable, and non-hazardous alternative. XG is a commonly used biopolymer in engineering. As a polysaccharide, XG is characterized by pseudoplasticity (recovery ability), exhibiting high viscosity even at low concentrations. Additionally, XG possesses high stability, being resistant to salts, enzymes, acids, and high temperatures[10,11]. Unlike traditional materials such as cement, XG is sustainable and environmentally friendly, making it a promising soil stabilization material[12]. Due to its thixotropic nature, XG experiences a rapid decrease in viscosity under shear stress, with higher shear rates leading to faster viscosity reduction. Once the shear stress is removed, the original viscosity is immediately restored. The main and side chains of XG contain numerous reactive functional groups, such as hydroxyl and carboxyl groups, which can be modified or functionalized through various methods, including physical and chemical modifications and hydrogel synthesis, to enhance its physicochemical properties and meet specific application requirements.

XG has been widely used in engineering in recent years, playing a significant role in the treatment of various soils such as silty soil, red clay, loess, and expansive soil, and has been widely applied due to its excellent performance[13–20]. Currently, numerous research achievements have been made in utilizing XG to modify soil. For instance, Singh et al.[20] investigated the plasticity and strength of highly expansive soil treated with XG and found that with the increase of XG content, the maximum dry density decreased, and the optimum moisture content increased. Wang Tianliang et al.[21] studied the modification of soil with XG and guar gum and showed that the shear strength increased by 150%-160%, and the compressive strength increased by 104.2%. Naveena et al.[22] indicated that the shear strength increased from 0.12 MPa to 1.98 MPa after modification, representing an increase of 1550%. Keshav et al.[23] studied the modification of soil with XG and guar gum and pointed out that the 28-day compressive strength increased by 630% at the XG content of 1%, with a corresponding decrease in the expansion rate of 45.45%. Weng et al.[24] investigated the solidification effect of XG on red clay with different dosages and curing times and showed that the compressive strength and cohesion of red clay increased by 93.31% and 79.47%, respectively, after 28 days of curing with an XG dosage of 1.5%. The aforementioned studies indicate that XG modification of soil mainly utilizes the pseudo-plastic water absorption of XG, i.e., XG combines with water to form a highly viscous gel, establishing a connecting bridge between soil particles that are not in direct contact, making the XG gel cover the surface of soil particles, increasing the viscosity between clay particles, and thus improving the strength and deformation resistance of the soil. Anisotropy plays a key role in how polymer bonding affects strength, as the directional properties of material structure and particle orientation influence polymer distribution within the material and bonding effectiveness. This leads to strength enhancement, with the highest gains typically observed in the polymer-strengthened direction. When molecular structures align with polymer chain orientations, intermolecular forces are enhanced, thereby improving bond strength[25,26].

In summary, although significant results have been achieved by utilizing the water absorption and high viscosity of XG to modify soil, numerous studies have focused on the mechanical properties and microscopic mechanisms of XG-modified expansive soil. Research on XG-modified red clay has been limited to mechanical properties, while a comprehensive and in-depth study on the mechanical fracture properties and microscopic pore characteristics under hydraulic erosion has not yet been conducted. Therefore, based on the pseudo-plastic modification of red clay with XG, this study investigated the mechanical properties, mechanical fracture properties under hydraulic erosion, and changes in microscopic pores of XG-modified red clay through compression tests, shear tests, dry-wet cycle tests, CBR tests, scanning electron microscopy (SEM), X-ray diffraction (XRD), and digital microscopic pore analysis. Based on the experimental results, suggested values for the optimal gum-soil ratio and curing time of XG-modified red clay were proposed to provide a numerical basis for the modification of red clay with XG and other biogums. The aim was to better and more comprehensively modify red clay, ensure a more rational utilization of XG performance, and thus provide a certain numerical basis for the application of biogums in geotechnical engineering to replace traditional soil modification methods.

Experimental materials and methods

Experimental materials

The red clay used in this study was collected from 0.75 to 1.5 m depth in a highway foundation pit in Hubei Province, China. The soil exhibited a reddish-brown color and a relatively uniform texture. The collected soil was air-dried at room temperature, crushed, and sieved through a 2 mm sieve to remove impurities, and then stored in a sealed container. The physical properties of the soil sample are presented in Table 1, and the particle size distribution curve is shown in Fig. 1. Approximately 86% of the soil particles were smaller than 0.075 mm, classifying the soil as fine-grained. The uniformity coefficient was 3.21, and the coefficient of curvature was 1.71, indicating a well-graded particle size distribution.

The xanthan gum (XG) used in this experiment was industrial-grade material sourced from Huafeng Powder Company (Fengqiu County, Henan Province). The XG appears as an off-white to light yellow powder, demonstrating stable viscosity across a broad temperature range (−98 °C to −90 °C). The material was odorless,

Natural moisture content (%)	Optimum moisture content (%)	Maximum dry density (g/cm^3)	Liquid limit (%)	Plastic limit (%)	Plasticity index (%)	Uniformity coefficient (%)	Curvature coefficient (%)
44.63	20.65	1.764	38.84	16.37	22.47	3.21	1.71

Table 1. Physical parameters of red clay.

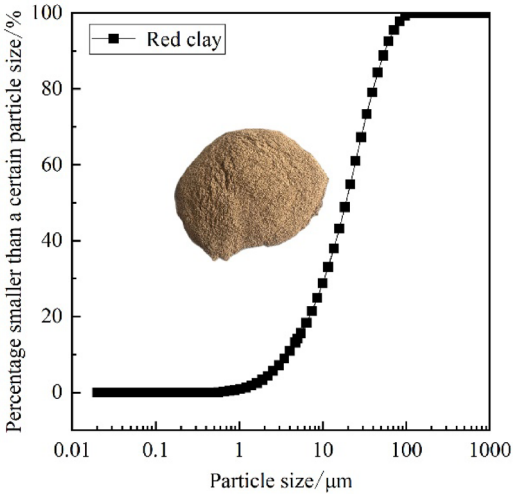

Fig. 1. Red clay vs. curve.

Molecular formula	Molecular weight	Loss on drying /%	Melting point/℃	Boiling point/℃	pH	Screening rate through 80 mesh/%
$C_{35}H_{49}O_{29}$	1×10^6g/mole	8.4	64.43	145.2	7.4	96.0

Table 2. XG basic physical parameters.

tasteless, and readily water-soluble. Key characteristics of the XG are summarized in Table 2, with the calcium oxide (CaO) content determined to be approximately 70% of the composition.

Experimental methods

Based on the results of preliminary tests, five XG dosage ratios (0%, 0.5%, 1%, 1.5%, and 2% by dry soil weight) were established. Prior to the experiment, the reserved soil samples were dry mixed with XG at predetermined ratios. Subsequently, distilled water was added to achieve the optimal moisture content, followed by thorough mixing. Thereafter, the mixture was allowed to hydrate for 24 h relative humidity before sample preparation. The methods for preparing samples subjected to wetting-drying cycles and shear strength tests were consistent.

Uniaxial compressive strength test

Uniaxial compressive strength tests were conducted using a microcomputer-controlled universal testing machine with a maximum load capacity of 20 kN and a loading rate of 1 mm/min. Tests were terminated when the stress-strain curve reached a peak. If no peak stress was observed, the test was stopped when the strain reached 20%. Specimens were prepared by statically compacting the soil into a standard mold with a height of 100 mm and a diameter of 50 mm.

Shear strength test

Direct shear tests were conducted using a four-jaw direct shear machine manufactured by Nanjing Soil Instrument Company. Normal stresses of 100 kPa, 200 kPa, 300 kPa, and 400 kPa were applied, with a shear rate set at 0.8 mm/min. Specimens were prepared by statically compacting the soil into a standard mold with a diameter of 61.8 mm and a height of 20 mm.

Wetting–drying cycle test

To simulate the highest ambient temperature in natural conditions, the 28-day cured samples were placed in an electrically heated drying oven at a constant temperature of 40 °C. One drying cycle lasted 24 h, followed by a rehydration period of 6 h. After each cycle, images of the sample fractures were captured to document the development of cracks. A total of four wetting-drying cycles were conducted.

California bearing ratio (CBR) test

The CBR test was performed using a TL127-II Road Material Strength Tester manufactured by Beijing Hongda Instrument Company. Test specimens were prepared using a heavy compaction apparatus. The specimen was placed on the lifting platform, and the control rod was adjusted to touch the specimen surface. A load of 45 N was applied to the penetration rod at a loading rate of 1 mm/min.

Microstructural testing

After 28 days of curing, soil samples from the center of the compressive strength specimens were collected, dried at low temperature, and ground into powder. The powder was then sieved through a 0.075 mm sieve and stored in sealed bags for subsequent use. For SEM analysis, the prepared soil samples were placed on conductive adhesive, subjected to freeze-drying (liquid nitrogen cooling under vacuum), and subsequently gold-sputtered to reduce electrical charging during imaging. The SEM analysis was performed using a field-emission scanning electron microscope (FESEM) produced by Hitachi, with an accelerating voltage ranging from 0.1 to 30 kV. XRD analysis was conducted using an Ultima X-ray diffractometer with the following parameters: linearity ≤ 0.030, resolution ≤ 0.130, repeatability ≤ 0.0020, 2θ angle ranging from 10° to 80°, scanning speed of 5°/min, and step width of 0.02.

Results analysis

Effect of XG on the compressive strength of red clay

Figure 2 presents the axial stress-strain curves of the modified soil. As shown in the figure, the compressive strength of the modified specimens can be categorized into three distinct phases based on the trend of the curves: rapid growth phase, slow growth phase, and slow decline phase[27,28]. Specifically, during the rapid growth phase, the increasing density of the modified specimens leads to a swift increase in compressive strength. In the slow growth phase, the stress gradually increases with increasing strain, and the compressive strength continues to rise until it reaches the peak strength. In the slow decline phase, the specimens begin to exhibit significant damage, causing the stress to drop rapidly and stabilize. With the extension of curing time, the stress-strain curves transition from strain-softening to strain-hardening behavior, with the uncured modified soil showing a more pronounced softening phenomenon.

Figure 3 presents the compressive strength of the modified soil. As shown in Fig. 3(a), the compressive strength initially increases and then decreases with the increase in XG dosage, reaching a peak value at an XG dosage of 1.5%. The growth of compressive strength varies significantly with different curing times. The compressive strength growth rates are 29.36 kPa/d from 0 to 7 days, 43.65 kPa/d from 7 to 14 days, and 62.23 kPa/d from 14 to 28 days. This indicates that the reaction between the modifier and soil is most rapid between 14 and 28 days. Prior to 14 days, XG and soil have not fully reacted, and the reaction slows down and stabilizes after 28 days. Figure 3(a) also shows that the modification effect of XG dosage on red clay is significant under the same curing time. For example, at 28 days of curing, the compressive strength reaches 437.94 kPa at an XG dosage of 1.5%, while other dosages result in lower strengths. When the XG dosage exceeds 1.5%, softening zones appear within the specimens, leading to a decrease in compressive strength. This suggests that there is an optimal XG dosage of 1.5%. The CaO in XG reacts chemically with the OH^- in the soil. Excessive XG dosage results in insufficient ion exchange by CaO, thereby inhibiting the enhancement of compressive strength. Figure 3(b) shows the compressive strength of modified soil at different curing times. It is evident that the compressive strength of all modified soils is higher than that of the uncured soil. After 28 days of curing, the compressive strength of the modified soil with 1.5% XG dosage increases by 99.46% compared to that of the unmodified soil.

Figure 4 illustrates the deformation modulus (E_{50}) of the modified red clay. As shown in Fig. 4(a), specifically, there is a critical value for the effect of different XG dosages on specimen deformation. After 28 days of curing, E_{50} is relatively high, but the ability of the modified soil to resist compressive deformation gradually decreases

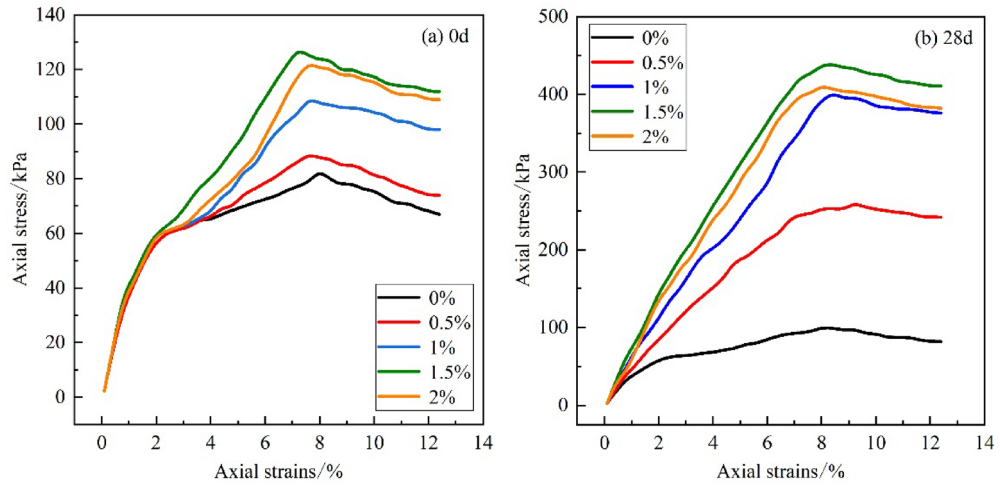

Fig. 2. Axial stress-strain curve of modified soil. (**a**) Cured for 0 d, (**b**) Cured for 28 d.

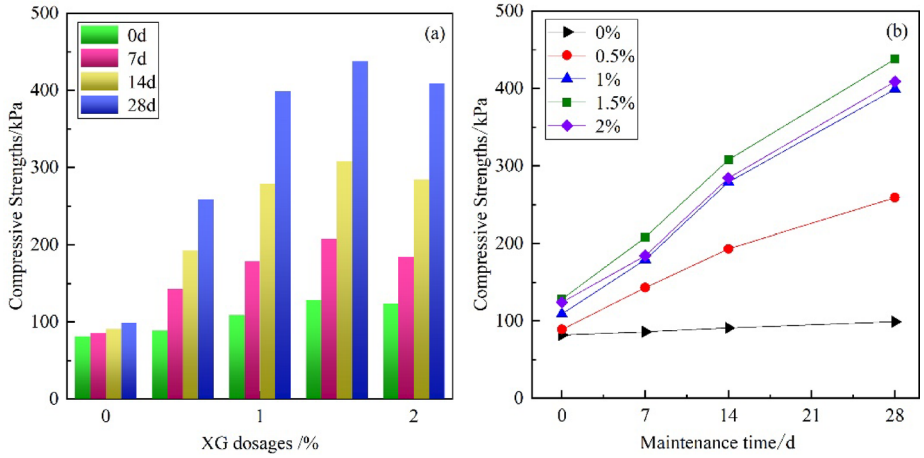

Fig. 3. Compressive strength of modified soil. (**a**) Different dosages, (**b**) Different curing periods.

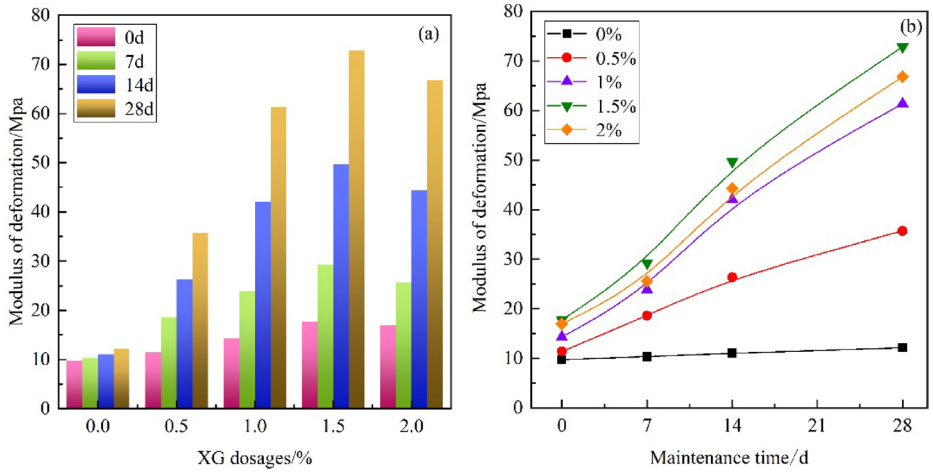

Fig. 4. Deformation modulus of modified soil. (**a**) Different dosages, (**b**) Different curing periods.

when XG dosage exceeds 1.5%. Figure 4(b) shows that E_{50} initially increases and then decreases with the increase in XG dosage, and it increases in a stepwise manner with curing time. The increases in E_{50} under different curing times are 74.13%, 59.54%, 75.06%, and 81.84%, respectively. After 28 days of curing, E_{50} increases by 7.71%, indicating a significant enhancement in the deformation resistance of the modified red clay, which also exhibits better ductility.

Effect of XG on the shear strength of red clay

Figure 5 illustrates the variation in shear strength of red clay modified by XG. As shown in the figure, the shear strength of the modified soil increases with the increment of normal stress. The shear strength of XG-modified soil increases approximately linearly with the increase in normal stress. For samples with the same curing time, the shear strength is maximized at an XG dosage of 1.5%, indicating that the addition of XG significantly enhances the shear strength of red clay. With the extension of curing time, the shear strength of the modified soil shows an upward trend. The shear strength increases by 1648.1%, 1968.4%, 2405.1%, 2900% at different curing times, with an increase rate exceeding 1600%.

As indicated by Fig. 5, the shear strength of the modified soil increases with curing time, with varying increments observed at different curing times. The experimental results reveal that the most significant increments in shear strength occur at 7 and 14 days of curing. Beyond 28 days of curing, the rate of increase in shear strength slows down and stabilizes. For XG-modified red clay, a curing time of at least 28 days is recommended.

Figure 6 illustrates the variations in cohesion and internal friction angle of the modified soil. As shown, the increase in XG dosage leads to a trend of first increasing and then decreasing in both cohesion and internal friction angle, with a peak value achieved at an XG dosage of 1.5%. This trend can be attributed to the dominant role of coarse particles on the surface of the specimens during shearing. Under shear stress, fine particles initially deform, forming interlocking mesh-like structures between particles. As the bonding effect of XG strengthens, the cohesion of the modified soil gradually increases, and the internal friction angle also rises. However, when

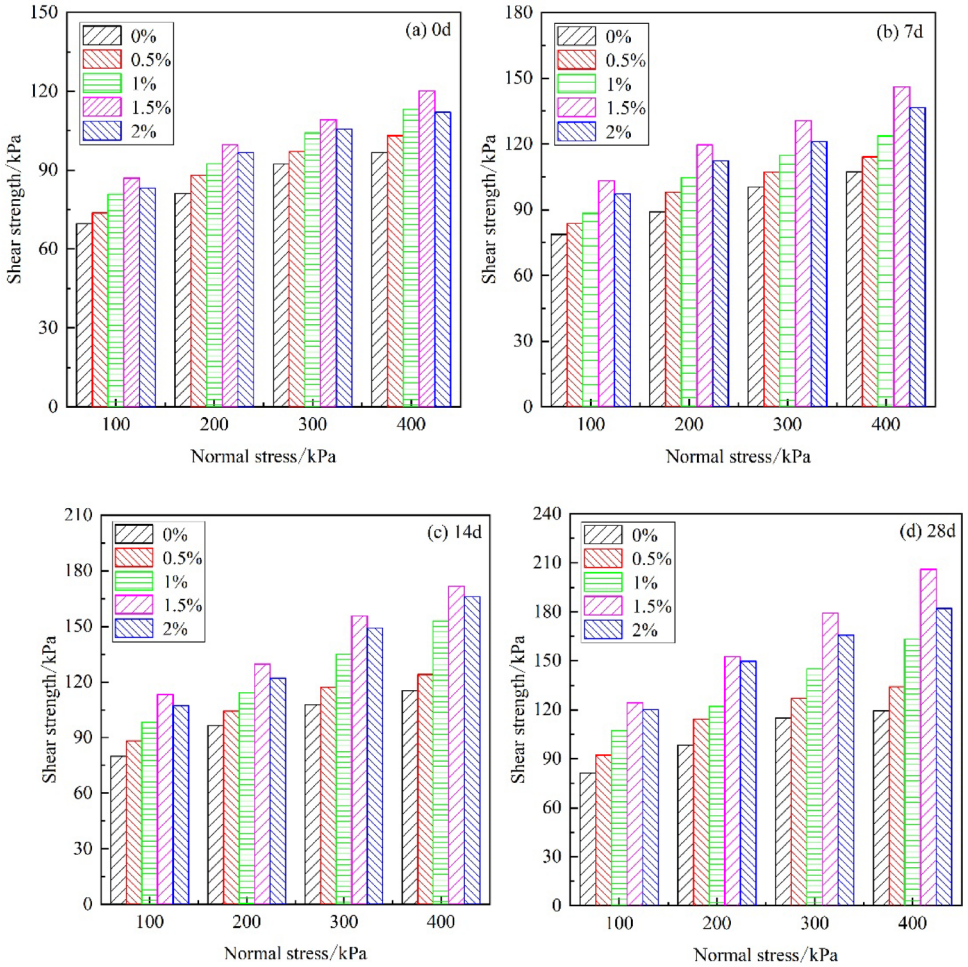

Fig. 5. Shear strength of modified soil. (**a**) Cured for 0 d, (**b**) Cured for 7 d, (**c**) Cured for 14 d, (**d**) Cured for 28 d.

the XG dosage exceeds 1.5%, excess XG fills the voids between particles, compromising the integrity of the specimens. In other words, once the XG dosage surpasses the critical value, the shear strength parameters of the modified soil exhibit a decreasing trend.

Effect of XG on the cracking behavior of modified soil

Figure 7 presents the crack patterns of modified soil subjected to wetting and drying cycles. As shown in Fig. 7(a), after two drying cycles, cracks of varying degrees appeared in the modified soil, while the unmodified soil exhibited significant shrinkage deformation. The modified soil developed secondary cracks in the center and edges, along with some primary cracks, whereas the unmodified soil had numerous primary cracks at the edges. This indicates that the gel membrane formed by XG could effectively inhibit crack development in the specimens. With increasing cycle numbers, the number of cracks gradually increased. In the unmodified soil, primary cracks became more pronounced and secondary cracks proliferated. After three wetting and drying cycles, the modified soil exhibited a more uniform crack distribution and better crack inhibition. At an XG dosage of 1.5%, the modified soil had numerous fine crack branches that penetrated the specimen surface. Additionally, it was observed that the surface crack patterns were influenced by the number of cycles. After four cycles, the cracks on the specimen surface increased and formed a mesh-like structure.

The digital image processing of the wetting-drying cycle crack images was conducted, and the geometric characteristics of the crack networks were analyzed using the PCAS (Photo-Crack Analysis System) software[29]. The digital image processing steps are as follows: (i) Grayscale conversion: Each pixel's RGB values were combined into a single grayscale value to enhance the contrast between cracks and soil. (ii) Binarization: A threshold was applied to convert the image into a binary format, with soil appearing as white and cracks as black. (iii) Noise removal: Noise points were identified and eliminated to avoid interference from non-crack black spots. (iv) Skeletonization: The skeletonization process extracted the morphological features of the crack networks without altering their shapes.

It can be observed from Fig. 8 that with increasing cycle numbers, the development of cracks in the modified soil slowed down, mainly characterized by the evolution of secondary cracks into primary cracks. The unmodified soil exhibited numerous primary cracks in the center and significant edge shrinkage and deformation. For the

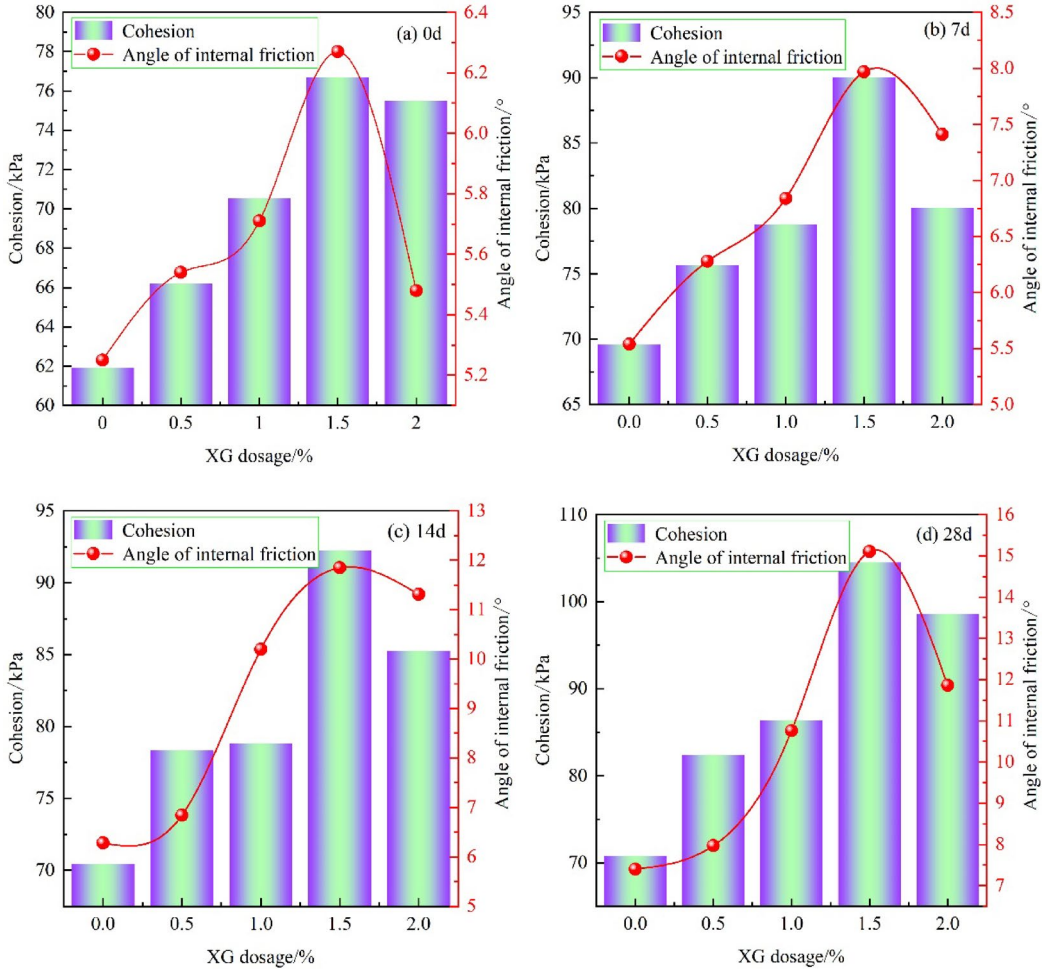

Fig. 6. Cohesion and internal friction angle of the modified soil. (**a**) Cured for 0 d, (**b**) Cured for 7 d, (**c**) Cured for 14 d, (**d**) Cured for 28 d.

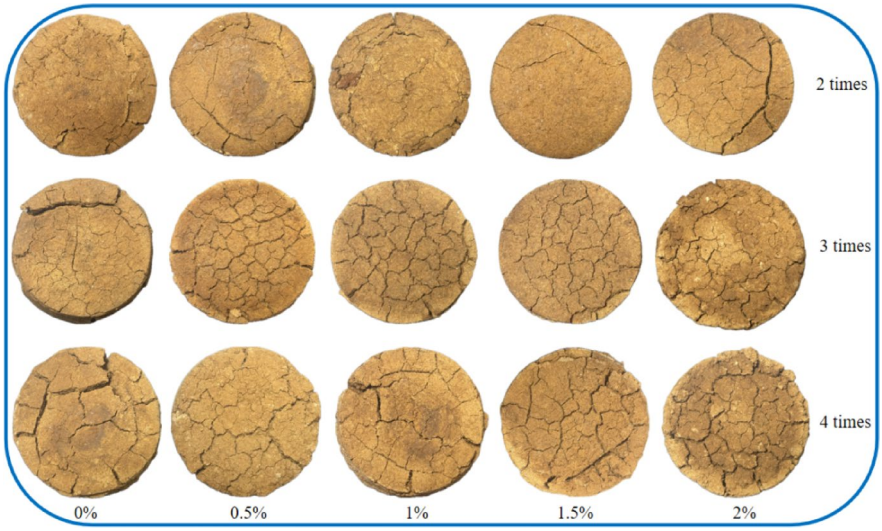

Fig. 7. Wetting-drying cycle crack images.

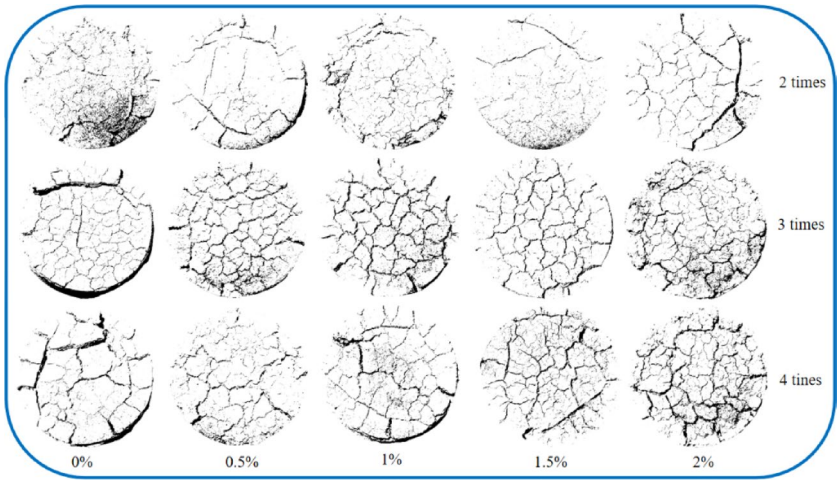

Fig. 8. Digitized image of fissure.

modified soil, the crack development was slowest at XG dosages between 1% and 1.5%. At lower XG dosages, the cracking behavior was similar to that of the unmodified soil. The optimal modification effect was achieved at an XG dosage of 1.5%, with only a few cracks appearing at the edges of the specimens. However, when the XG dosage exceeded 1.5%, the cracking was more pronounced, dominated by primary cracks.

Effect of wetting–drying cycles on mechanical properties

Figure 9 presents the shear strength of modified soil under wetting-drying cycles. Results indicate that the shear strength of modified soil gradually decreases with increasing cycle numbers. However, the shear strength of XG-modified soil remains higher than that of unmodified soil, indicating the effectiveness of XG in enhancing the soil's resistance to hydraulic erosion through gelation. Additionally, under the same number of cycles, the shear strength significantly increases with increasing normal stress. This can be attributed to the gel membrane formed by XG within the soil matrix, which enhances the soil's resistance to hydraulic erosion. The rate of shear strength reduction decreases with increasing cycle numbers, suggesting that the gel membrane gradually stabilizes under repeated wetting-drying cycles.

Figure 10 presents the cohesion and internal friction angle of modified soil under different numbers of wetting-drying cycles. The results indicate that both cohesion and internal friction angle of the modified soil gradually decrease with increasing cycle numbers. However, the reduction in internal friction angle is relatively smaller when compared to that of cohesion. After two cycles, the rate of decline in shear strength parameters becomes slower, primarily due to the water absorption of XG, which causes the soil to dry and crack, leading to structural damage. Lee et al.[30] reported that XG exhibits relatively stable cohesion under alternating wetting and drying conditions, which is consistent with the findings in this study.

Figure 11 presents the compressive strength of modified soil under different numbers of wetting-drying cycles. The results show that the compressive strength of modified soil decreases with increasing cycle numbers. However, the addition of XG improves the mechanical properties of red clay. After cycling, the compressive strength of modified soil remains higher than that of unmodified soil, indicating that XG enhances the soil's resistance to hydraulic erosion. The significant reduction in compressive strength of modified soil indicates the formation of van der Waals forces during the wetting-drying cycles. These forces aggregate the free fine particles into larger aggregates, strengthening the soil's coarse particle framework and reducing the specific surface area of the particles. This results in larger inter-particle voids, which lead to a decrease in strength under hydraulic erosion[30]. As the number of cycles increases, the van der Waals forces stabilize, and the rate of compressive strength reduction slows down. The attenuation is more pronounced at XG dosages of 1.5% and 2%, indicating that these concentrations are more susceptible to structural damage under repeated cycles.

Effect of XG on the CBR of modified soil

Figure 12 presents the CBR values of the modified soil. As shown in Fig. 12(a), the CBR initially increases with increasing XG dosage and then decreases. The optimal modification effect was achieved after 28 days of curing, with the peak CBR value reaching 24.1%. Subsequently, the CBR decreases gradually as the XG dosage increases beyond 1.5%, which is consistent with the trend observed in the compressive strength. The growth rates of CBR after 7, 14, and 28 days of curing were 106.97%, 158.14%, and 230.23%, respectively, indicating a significant improvement in CBR after XG modification. After 7 days of curing, the CBR of all modified soils exceeded 8%, meeting the engineering standards for first-class highways[31]. After 28 days of curing, the CBR increases to 24.1% with a 1% XG dosage, and the maximum CBR at a 1.5% dosage is 5.58 times that of the unmodified soil, showing a remarkable modification effect. It can also be found that the CBR first increases and then decreases with the increase in XG dosage, with 1.5% being the critical dosage, after which it decreases rapidly, which is consistent with the research results[32].

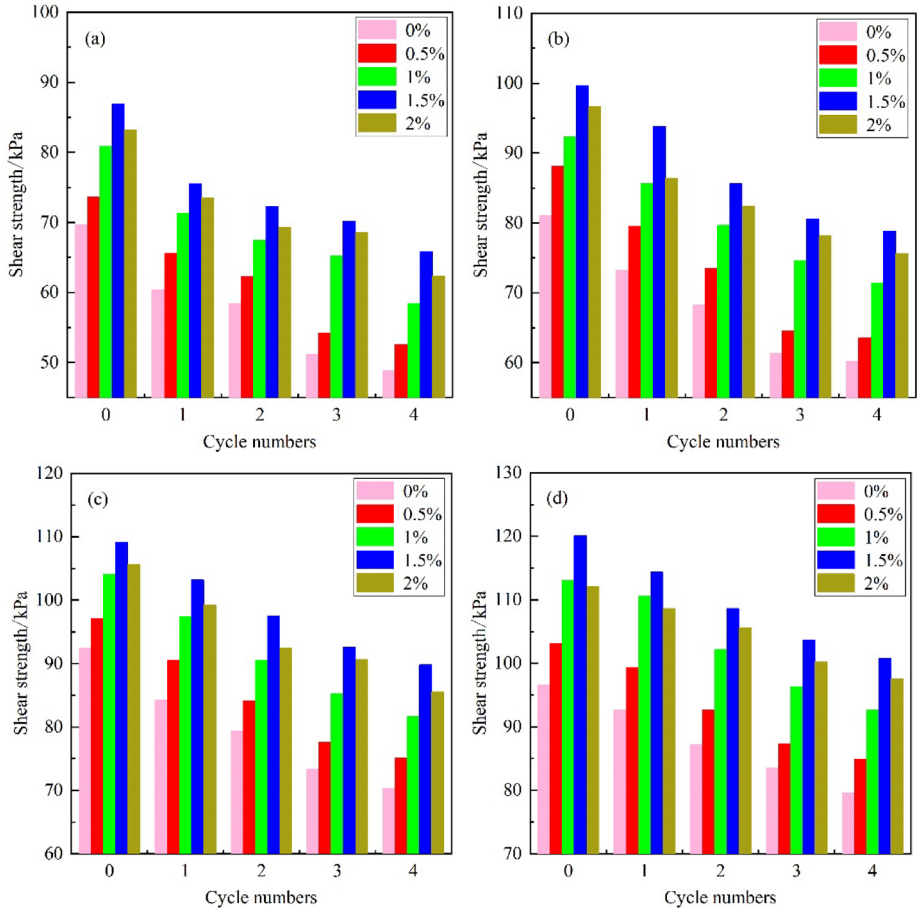

Fig. 9. Shear strength of modified soil under wetting-drying cycles. (**a**) Normal Stress 100 kPa, (**b**) Normal Stress 200 kPa, (**c**) Normal Stress 300 kPa, (**d**) Normal Stress 400 kPa.

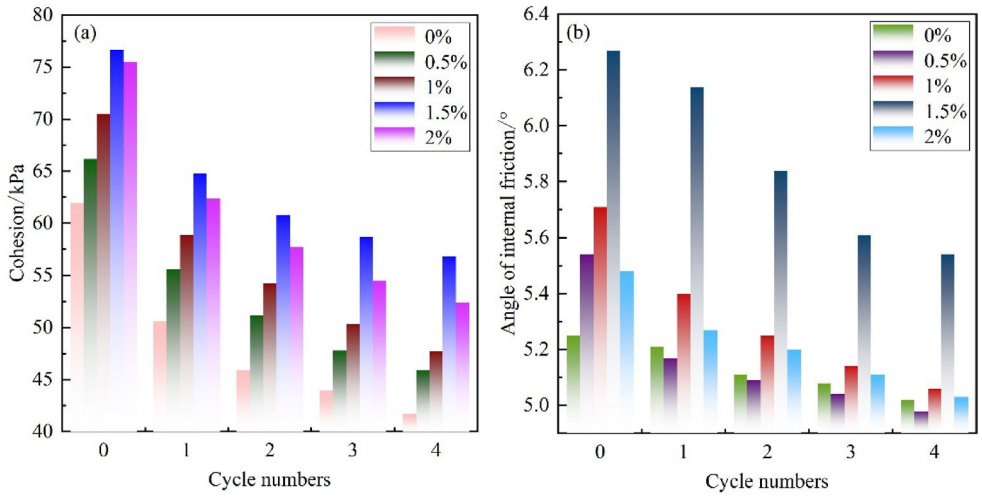

Fig. 10. Cohesion and angle of internal friction of consolidated soils with different number of cycles. (**a**) Cohesion, (**b**) Internal friction angle.

As shown in Fig. 12(b), the modified soil with an XG dosage of 1.5% exhibits the highest CBR value, and the modification effect improved with increasing curing time. The CBR of the modified soil initially increases rapidly with the XG dosage and then decreases after exceeding 1.5%, which can be attributed to the fact that the bearing capacity of this type of modified soil is mainly provided by cohesion[33]. Consequently, CBR also follows

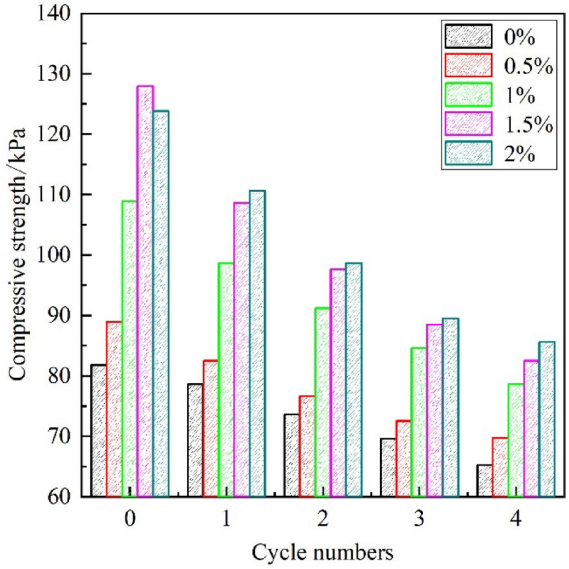

Fig. 11. Compressive strength of modified soil with different number of cycles.

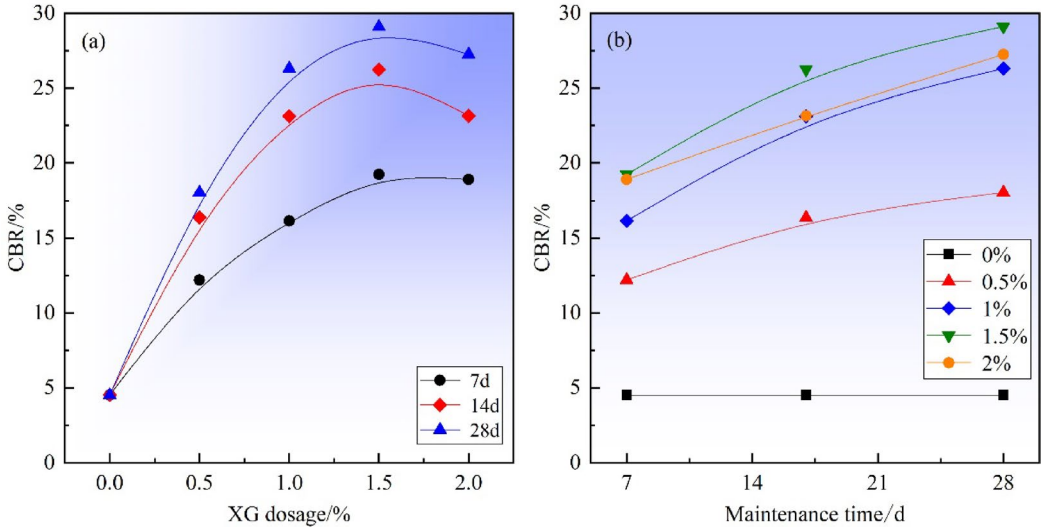

Fig. 12. CBR values of XG-modified soil. (**a**) Different dosages, (**b**) Different curing periods.

the same trend with an increase in XG dosage. The continuous increase in CBR with the extension of curing time indicates that chemical reactions continue to occur within the modified soil samples even after 28 days, leading to the growth of CBR.

Effect of XG on the microstructural features of modified soil

Figure 13 presents the SEM images of the experimental materials. Figure 13(a) shows the microstructural features of XG at a magnification of 500 times. It is observed that XG has a double-layered tubular structure with a smooth and light surface, irregular shape, and large specific surface area. Additionally, some XG tubules exhibit a hollow interior, and there are some flaky debris.

Figure 13(b) presents the scanning electron microscopy (SEM) image of the unmodified red clay at a magnification of 5000 times. The unmodified soil particles are observed to be loosely packed with large pores, indicating poor inter-particle bonding and consequently low soil strength. Figure 13c–e show the SEM images of the XG-modified red clay at the same magnification. Compared with the unmodified soil, the modified soil particles exhibit a rougher surface, reduced porosity, and a coating of a binder-gel film. The inter-particle connections are significantly enhanced, resulting in the formation of numerous aggregates and improved soil stability. Additionally, some flaky or needle-like hydration products envelop the soil particles, obscuring the particle boundaries. It is observed that with the increase in XG dosage, the amount of hydration gel increases. These needle-like gels enhance the adhesion between particles through connection, while some of the gel fills the

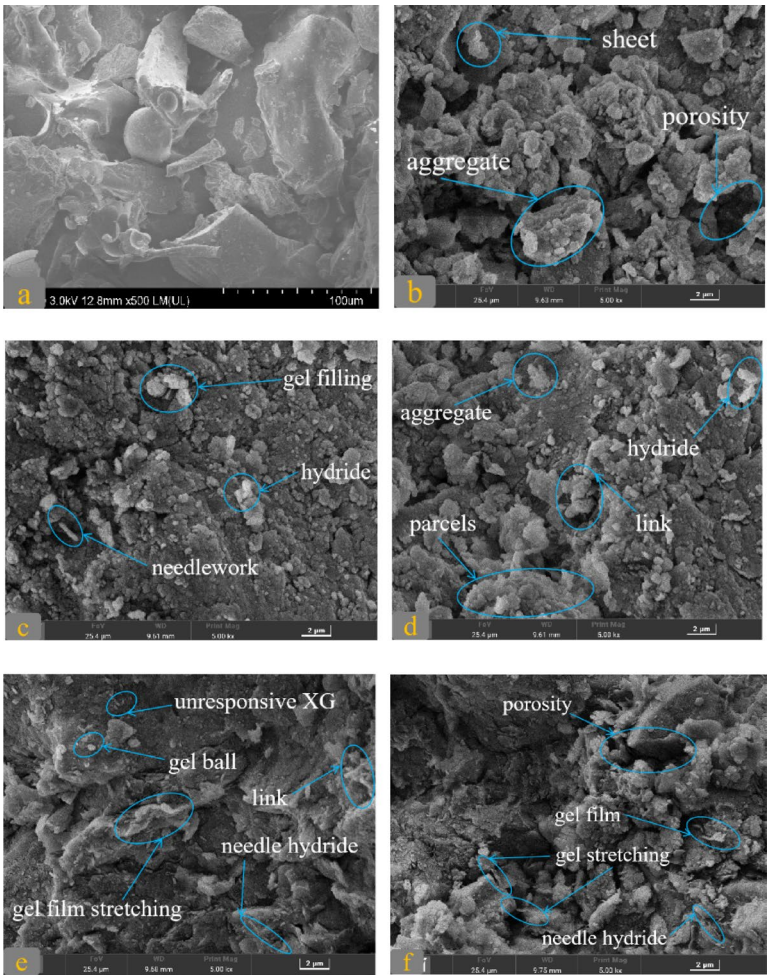

Fig. 13. SEM test images. (**a**) XG, (**b**) 0% XG dosage, (**c**) 0.5% XG dosage, (**d**) 1% XG dosage, (**e**) 1.5% XG dosage, (**f**) 2% XG dosage.

pores to densify the soil structure. The binding effect of XG promotes the formation of stable aggregates, leading to a significant increase in macroscopic strength.

Figure 14 presents the X-ray diffraction (XRD) patterns of the XG-modified soil. The unmodified soil is primarily composed of quartz and some hydrophilic minerals. After XG modification, no new mineral phases were detected, and the peak shapes in the XRD patterns remained relatively unchanged. However, after 28 days of curing, the dosage of hydrophilic minerals such as montmorillonite and illite decreased significantly by 32.57% and 21.42%, respectively. Due to the limitations of sample selection and the focus on the central part of the specimens after the compressive tests, it cannot be conclusively stated that the hydrophilic minerals completely disappeared. However, it is evident that the dosage of hydrophilic minerals was reduced after 28 days of modification.

Combined SEM and XRD analyses indicate that the formation of the gel film is primarily attributed to hydration reactions. Due to the presence of SiO_2 in red clay, silicate particles are formed upon contact with water, leading to the intercalation of K^+ and Na^+ ions between the crystal layers[34]. Meanwhile, XG contains a large amount of CaO, which dissociates in aqueous solutions to release a significant amount of Ca^{2+} ions. Owing to its strong attraction, Ca^{2+} ions can replace K^+ and Na^+ ions through ion exchange[35]. The substitution of Ca^{2+} for K^+ and Na^+ enhances the inter-layer bonding, leading to the formation of a gel film around the soil particles and the development of aggregates, which explains the observed decrease in hydrophilic minerals. Additionally, when the concentration of Ca^{2+} ions in the solution exceeds the demand for ion exchange, the excess Ca^{2+} ions can react with SiO_2 and Al_2O_3 in the clay minerals to form amorphous calcium silicate (C-S-H) and calcium aluminate (C-A-H) hydrates, as detailed in the literature[36]. SEM analysis confirms the formation of amorphous hydrates (gel film on soil particles, gel spheres), which enhance the strength of the modified red clay through tensile, enveloping, and filling mechanisms.

To quantitatively analyze the particle distribution and pore arrangement in the modified soil, directional probability entropy, fractal dimension, and shape factor were introduced. Directional probability entropy reflects the orientation of soil pores, with higher values indicating more random pore arrangement. Fractal dimension quantifies the irregularity of complex shapes and reflects the efficiency with which a complex shape occupies

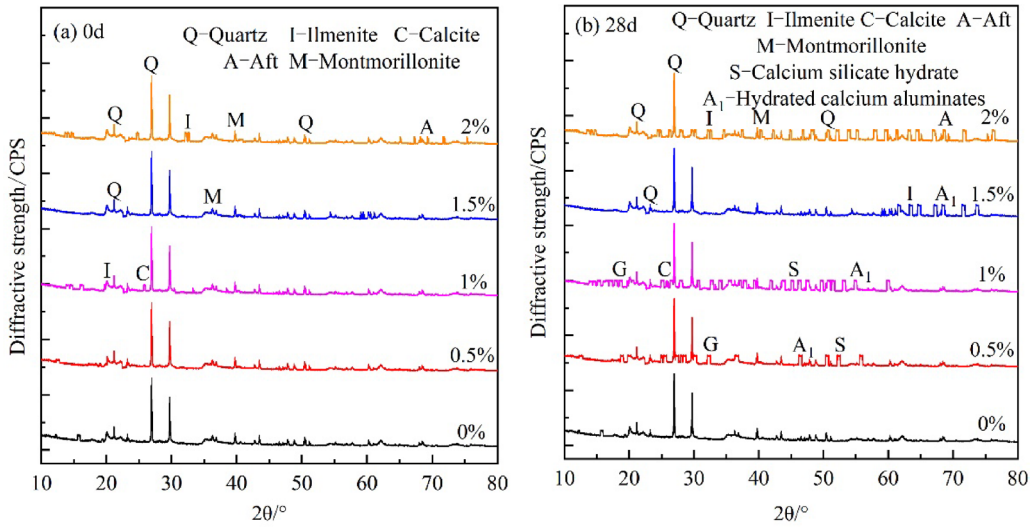

Fig. 14. XRD patterns of XG-modified soil. (**a**) Cured for 0 d, (**b**) Cured for 28 d.

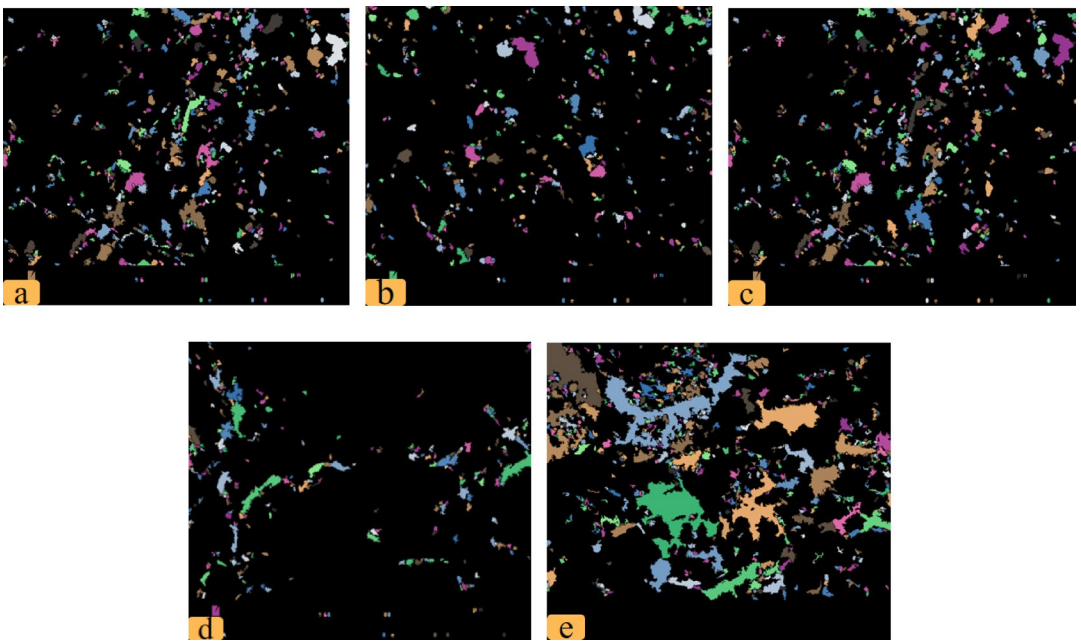

Fig. 15. SEM images processed by PCAS. (**a**) 0% XG dosage, (**b**) 0.5% XG dosage, (**c**) 1% XG dosage, (**d**) 1.5% XG dosage, (**e**) 2% XG dosage.

space. Shape factor indicates the influence of material shape on its density. Based on the pore analysis system PCAS software V2.325 developed by Nanjing University and using the research methods in the literature[35,37], the SEM images of the modified soil were processed to extract pore information. The results of threshold segmentation of the SEM images are shown in Fig. 15. The pore parameters of the modified soil with different XG dosages were statistically analyzed after 28 days of curing, and the results are presented in Table 3.

As shown in Table 3, the directional probability entropy of the modified soil with different XG dosages is generally close to 1, indicating no significant directional distribution of pores. The shape factors of all samples showed no obvious change after modification, suggesting a certain degree of complexity and similarity in the microstructure of the modified soil, which further confirms the relatively dense internal structure of the modified soil. Additionally, the fractal dimension of the modified soil did not vary significantly, reaching a maximum at an XG dosage of 1.5%. The porosity of the modified soil initially decreased and then increased with the increase in XG dosage, reaching a minimum at an XG dosage of 1.5%, indicating that the soil structure was the best at this dosage.

Dosage/%	Oriented probability entropy	Fractal dimension	Shape factor	Porosity/%	Average pixel area
0	0.992	1.23	0.47	21.34	283.34
0.5	0.987	1.25	0.44	19.52	300.45
1	0.989	1.22	0.43	17.63	346.53
1.5	0.990	1.26	0.41	17.32	372.21
2	0.991	1.21	0.42	18.25	369.82

Table 3. Statistics of PCAS pore parameters of modified soil.

Conclusion

Through laboratory tests on XG-modified red clay, this study investigated the effects of XG on the mechanical and microstructural properties of red clay and elucidated the underlying mechanisms of XG modification. The evolution of porosity in the modified soil was analyzed using pore analysis software. The main conclusions are as follows:

(1) The shear strength of the modified soil increases approximately linearly with the increase in normal stress, reaching a peak at an XG dosage of 1.5%. Both cohesion and internal friction angle first increase and then decrease with increasing XG dosage, reaching their maxima at an XG dosage of 1.5%.
(2) The compressive strength increases first and then decreases with increasing XG dosage, with the fastest strength gain observed between 14 and 28 days of curing. The E_{50} value of the modified soil first increases and then decreases with increasing XG dosage and exhibits a stepwise increase with curing time. The E_{50} value increased by 7.71% after 28 days of curing.
(3) Crack development in the modified soil proceeded slowly with increasing numbers of cycles, and secondary cracks evolved into primary cracks. The unmodified soil exhibited more primary cracks in the middle and larger shrinkage cracks at the edges. The shear strength of the modified soil showed a decreasing trend after wet-dry cycles, and both cohesion and internal friction angle gradually decreased with increasing numbers of cycles. The compressive strength of the modified soil also showed a weakening trend with increasing numbers of cycles.
(4) The CBR of the modified soil initially increased and then decreased with an increase in XG dosage, reaching a peak value of 24.1% at an XG dosage of 1.5%, after which it declined. The CBR growth rates after curing for 7, 14, and 28 days were 106.97%, 158.14%, and 230.23%, respectively. The CBR value of the soil modified with 1.5% XG after 28 days of curing was 5.58 times that of the unmodified soil, demonstrating a significant modification effect.
(5) The addition of XG resulted in the formation of flaky/needle-like gels, which enhanced the soil structure by filling, tensile, and enveloping mechanisms, leading to the formation of denser aggregates. No new minerals were formed after XG modification, but the dosage of hydrophilic minerals decreased significantly by 53.99%. The average and total porosity of the soil decreased with the addition of XG but increased when the XG dosage exceeded 1.5%.

Data availability

The datasets used during this study are available from the corresponding authors upon reasonable request.

Received: 21 March 2025; Accepted: 14 August 2025
Published online: 29 August 2025

References

1. He, Y. et al. Shear strength of high liquid limit red clay contaminated by diesel oil. *J. Railw. Sci. Eng.* **19**(03), 691–696 (2022).
2. Zhao, X. et al. Experimental study on fully weathered phyllite composite improved soil and numerical analysis of subgrade settlement. *J. Railw. Sci. Eng.* **20**(02), 554–564 (2023).
3. Yang, Y. et al. The influence of irreversibility of desiccation of lateritic soils on their physico mechanical properties. *Chin. J. Geotech. Eng.* **04**, 104–113 (1982).
4. Tan, Y. et al. Pore size evolution of compacted laterite under desiccation shrinkage process effects. *Rock Soil Mech.* **36**(02), 369–375 (2015).
5. Cao, H. et al. Experimental study of pavement performances of lime-treated laterite soil considering drying-wetting cycle paths. *Rock Soil Mech.* **33**(09), 2619–2624 (2012).
6. You, Q. et al. Strength properties of ionic soil stabilizer treated red soil. *China J. Highw. Transp.* **32**(05), 64–71 (2019).
7. Zeng, J. Experimental study on improvement of red clay with lime. *J. Railw. Sci. Eng.* **13**(07), 1289–1293 (2016).
8. Fu, X. et al. Experimental study about mechanic and permeability of soil-cement in different pH value. *J. Railw. Sci. Eng.* **14**(08), 1639–1646 (2017).
9. Ruan, B. et al. Experimental study on unconfined compressive strength of glass fiber reinforced lime soil. *J. Railw. Sci. Eng.* **15**(09), 2246–2251 (2018).
10. Cao, Z. et al. Effect of xanthan gum and paim silk fiber on compressive strength of Shanghai clay. *J. Water Resour. Water Eng.* **30**(05), 209–214 (2019).
11. Zhou, S. et al. Research development the structure property and application of xanthan gum. *Food Sci. Technol.* **33**(7), 156–160 (2008).
12. Roy, A. et al. Hydrophobically modified xanthan: an amphiphilic but not associative polymer. *Bio-macromolecules* **15**(4), 1160–1170 (2014).
13. Zhang, J. et al. Water retention characteristics of silt improved by three types of biopolymers. *Rock Soil Mech.* **43**(8), 2157–2164 (2022).

14. Zuo, C. et al. Experimental study on loess compressive strength improvement through xanthan gum and basalt fiber. *Coal Geol. China* **34**(01), 575–61 (2022).
15. Barani, O. R. et al. Effect of xanthan gum biopolymer on fracture properties of clay. *J. Mater. Civil Eng.* **33**(1), 04020426 (2021).
16. Zhang, S. et al. Strength improvement and microscopic mechanisms of tailings sands using xanthan gum and guar gum. *J. Eng. Geol.* **31**(2), 441–448 (2023).
17. Zhang, J. et al. Dynamic strength characteristics and microscopic analysis of silt improved by xanthan gum. *J. Basic Sci. Eng.* **11**(18), 1–11 (2023).
18. Wei, S. et al. Study on unconfined compressive strength and strengthening mechanism of xanthan gum modified clay. *J. Hebei Univ. Eng.* **38**(02), 66–71 (2021).
19. Song, Z. et al. Strength characteristics of biopolymer modified sand under dry-wet cycle. *Acta Mater. Compos. Sin.* **40**(04), 2285–2295 (2023).
20. Singh, S. P. et al. Plasticity and strength characteristics of expansive soil treated with xanthan gum biopolymer. *Probl. Soils Geoenviron. Concerns* **1**, 649–663 (2020).
21. Wang, T. et al. Experimental study on mechanical properties of expansive soil improved by xanthan gum and guar gum. *China Railw. Sci.* **44**(02), 1–10 (2023).
22. Naveena, S. et al. Strength characteristics of expansive soils using eco-friendly xanthan gum. *Int. J. Sci. Res.* **6**(06), 2319–7064 (2017).
23. Keshav, N. et al. *Enhancing the Properties of Expansive Soil Using Biopolymers-Xanthan Gum and Guar Gum* 129–135 (2019).
24. Weng, Z. et al. Mechanical behavior and strengthening mechanism of red clay solidified. *J. Central S. Univ.* **30**(06), 1948–1963 (2023).
25. Al-Rkaby, J. H. A. et al. Stress and deformation characteristics of nonwoven geotextile reinforced sand under different directions of principal stress. *Int. J. Geosynth. Ground Eng.* **3**, 4 (2017).
26. Rkaby, A. J. H. A. et al. An experimental study on the cyclic settlement of sand and cemented sand under different inclinations of the bedding angle and loading amplitudes. *Eur. J. Environ. Civil Eng.* **23**(8), 971–986 (2017).
27. Basha, E. A. et al. Stabilization of residual soil with rice husk ash and cement. *Constr. Build. Mater.* **19**(6), 448–453 (2005).
28. Liu, Y. et al. Stabilization of expansive soil using cementing material from rice husk ash and calcium carbide residue. *Constr. Build. Mater.* **221**, 1–11 (2019).
29. Lu, C. et al. Study on macro- and micro-scale properties of fiber reinforced red clay based on NMR and unconfined compressive strength tests. *J. Railw. Sci. Eng.* **18**(08), 2066–2072 (2021).
30. Lee, S. J. et al. Geotechnical shear behavior of xanthan gum biopolymer treated sand from direct shear testing. *Geomech. Eng.* **12**, 831–847 (2017).
31. PRC Ministry of Transport. *Design Guidelines for Highway Subgrade JTG D30–2019* (People's Transportation Press, 2019).
32. Nagarj, H. B. et al. Influence of clay mineralogy on the relationship of CBR of fine-grained soils with their Index and Engineering properties. *Transp. Geotech.* **1**, S2214391217301654 (2018).
33. Ma, Q. et al. Strength characteristics and micro-scale mechanism of high liquid limit clay treated by recycled construction and demolition wastes (CDW) aggregates. *Constr. Build. Mater.* **332**, 127367 (2022).
34. Xu, P. et al. The mineral physics characteristics of crystal structure and water structure in the montmorillonite. *Northwest Geosci.* **32**, 14–32 (1991).
35. Li, L. et al. Study on mechanical and microscopic characterization of expensive soil solidified by rice husk ash-granulated blast furnaxe slag. *Rock Soil Mech.* **44**(10), 2821–2832 (2023).
36. Liu, Y. *Study on Mechanism and Physical-Mechanical Properties of Stabilized Expansive Soil by Cementitious Material from Calcium Carbide Residue and Rice Husk Ash* (China University of Mining and Technology, 2019).
37. Liu, C. et al. Digital image recognition method of rock particle and pore system and its application. *Chin. J. Geotech. Eng.* **40**(5), 925–931 (2018).

Acknowledgements

The authors want to thank the editor and anonymous reviewers for their valuable suggestions for improving this paper.

Author contributions

Conceptualization, F.Y. and W.N.; methodology, W.N.; software, W.N. and Y.L.; validation, W.N.; formal analysis, Y.L.; investigation, Z.Z.; resources, W.N.; data curation, W.N.; writing—original draft preparation, W.N. and Z.J.; writing—review and editing, F.S.; visualization, W.N.; supervision, F.S.; project administration, W.N. and H.D.; funding acquisition, W.N. All authors have read and agreed to the published version of the manuscript.

Declarations

Competing interests

The authors declare no competing interests.

Additional information

Correspondence and requests for materials should be addressed to Z.Z. or W.N.

Reprints and permissions information is available at www.nature.com/reprints.

Publisher's note Springer Nature remains neutral with regard to jurisdictional claims in published maps and institutional affiliations.